
GNN-DT: A Graph Neural Network Enhanced Decision Transformer for Efficient Optimization in Dynamic Environments

Stavros Orfanoudakis, Nanda Kishor Panda, Peter Palensky, Pedro P. Vergara

Electrical Engineering, Mathematics and Computer Science

Delft University of Technology, The Netherlands

{s.orfanoudakis, n.k.panda, p.palensky, p.p.vergarabarrios}@tudelft.nl

Abstract

Reinforcement Learning (RL) methods used for solving real-world optimization problems often involve dynamic state-action spaces, larger scale, and sparse rewards, leading to significant challenges in convergence, scalability, and efficient exploration of the solution space. This study introduces GNN-DT, a novel Decision Transformer (DT) architecture that integrates Graph Neural Network (GNN) embedders with a novel residual connection between input and output tokens crucial for handling dynamic environments. By learning from previously collected trajectories, GNN-DT tackles the sparse rewards limitations of online RL algorithms and delivers high-quality solutions in real-time. We evaluate GNN-DT on the complex electric vehicle (EV) charging optimization problem and prove that its performance is superior and requires significantly fewer training trajectories, thus improving sample efficiency compared to existing DT and offline RL baselines. Furthermore, GNN-DT exhibits robust generalization to unseen environments and larger action spaces, addressing a critical gap in prior offline and online RL approaches.

1 Introduction

Sequential decision-making problems are critical for efficiently operating a wide array of industries, such as power systems control [1], logistics optimization [2], portfolio management [3], and advanced manufacturing processes [4]. However, many practical problems, such as the electric vehicle (EV) charging optimization [5], are large-scale, have temporal dependencies, and aggregated constraints, often making conventional methods impractical [6]. This is especially observed in dynamic environments, where the optimization landscape continuously evolves, requiring real-time solutions.

Reinforcement learning (RL) [7] has been extensively studied for solving optimization problems due to its ability to manage uncertainty, adapt to dynamic environments, and enhance decision-making through trial-and-error [8, 9]. In complex and large-scale scenarios, RL can provide high-quality solutions in real-time compared to traditional mathematical programming techniques that fail to do so [10]. However, RL approaches face significant challenges, such as sparse reward signals that slow learning and hinder convergence to optimal policies [11]. In addition, RL solutions struggle to generalize when deployed in environments different from the one they were trained in, limiting their applicability in real-world scenarios with constantly changing conditions [12].

Decision Transformers (DT) [13] is an offline RL algorithm that reframes traditional RL problems as generative sequence modeling tasks conditioned on future rewards [14]. By learning from historical data, DTs effectively address the sparse reward issue inherent in online RL, relying on demonstrated successful outcomes instead of extensive trial-and-error exploration. However, the trajectory-stitching mechanism of DT often proves insufficient in dynamic real-world environments, leading to suboptimal

policies. Although improved variants such as Q-regularized DT (Q-DT) [15] incorporate additional constraints for greater robustness, they still face significant challenges in generalizing across non-stationary tasks [16]. Consequently, further architectural advances and training strategies are essential to ensure consistent performance in complex environments.

This study introduces GNN-DT¹, a novel DT architecture that leverages the permutation-equivariant properties of Graph Neural Networks (GNNs) to handle dynamically changing state-action spaces (i.e., varying numbers of nodes over time) and improve generalization. By generating embeddings that remain consistent under node reordering, GNNs offer a powerful way to capture relational information in complex dynamic environments. Moreover, GNN-DT features a novel residual connection between input and output tokens, ensuring that action outputs are informed by the dynamically learned state embeddings for more robust decision-making. To demonstrate the superior performance of the proposed method, we conduct extensive experiments on the complex multi-objective EV charging optimization problem [17], which encompasses sparse rewards, temporal dependencies, and aggregated constraints. The main contributions are summarized as follows:

- Introducing a novel DT architecture integrating GNN embeddings, resulting in enhanced sample efficiency, superior performance, robust generalization to unseen environments, and effective scalability to larger action spaces, demonstrating the critical role of GNNs.
- Demonstrating that online and offline RL baselines, even when trained on diverse datasets (Optimal, Random, Business-as-Usual) with varying sample sizes, perform inferior to GNN-DT when dealing with real-world optimization tasks.
- Proving that both the size and type of training dataset critically influence the learning process of DTs, highlighting the importance of dataset selection. Also, shown that strategically integrating high- and low-quality training data (Optimal & Random datasets) significantly enhances policy learning, outperforming models trained exclusively on single-policy datasets.

2 Related Work

Advancements in Decision Transformers Classic DT encounters significant challenges, including limited trajectory stitching capabilities and difficulties in adapting to online environments. To address these issues, several enhancements have been proposed. The Q-DT [15] improves the ability to derive optimal policies from sub-optimal trajectories by relabeling return-to-go values in the training data. Elastic DT [18] enhances classic DT by enabling trajectory stitching during action inference at test time, while Multi-Game DT [19] advances its task generalization capabilities. The Online DT [20, 21] extends DTs to online settings by combining offline pretraining with online fine-tuning, facilitating continuous policy updates in dynamic environments. Additionally, adaptations for offline safe RL incorporate cost tokens alongside rewards [22, 23]. DT has also been effectively applied to real-world domains, such as healthcare [14] and chip design [24], showcasing its practical utility.

RL for EV Smart Charging RL algorithms offer notable advantages for EV dispatch, including the ability to handle nonlinear models, robustly quantify uncertainty, and deliver faster computation than traditional mathematical programming [25]. Popular methods, such as DDPG [26], SAC [27], and batch RL [28], show promise but often lack formal constraint satisfaction guarantees and struggle to scale with high-dimensional state-action spaces [29, 30]. Safe RL frameworks address these drawbacks by imposing constraints via constrained MDPs, but typically sacrifice performance and scalability [31, 32]. Multiagent RL techniques distribute complexity across multiple agents, e.g., charging points, stations, or aggregators [33], yet still encounter convergence challenges and may underperform in large-scale applications. To the best of our knowledge, no study has used DTs to solve the complex EV charging problem, despite DTs’ potential to handle sparse rewards effectively.

3 Preliminaries

In this section, an introduction to offline RL and the mathematical formulation of the EV charging optimization problem is presented as an example of what type of problems can be solved by the proposed GNN-DT methodology.

¹The code can be found at <https://github.com/StavrosOrf/DT4EVs>.

3.1 Offline RL

Offline RL aims to learn a policy $\pi_\theta(a | s)$ that maximizes the expected discounted return $\mathbb{E}[\sum_{t=0}^{\infty} \gamma^t R(s_t, a_t)]$ without additional interactions with the environment [34]. A Markov Decision Process (MDP) is defined by the tuple (S, A, P, R, γ) , where S is the state space, A the action space, P the transition function, R the reward function, $\gamma \in (0, 1]$ the discount factor [7]. In the offline setting, a static dataset $\mathcal{D} = \{(s, a, r)\}$, collected by a (potentially suboptimal) policy, is provided. DTs leverage this dataset by treating RL trajectories as sequences, learning to predict actions that maximize returns based on previously collected experiences. A key component in DTs is the *return-to-go* (RTG), which for a time step t can be defined as: $G_t = \sum_{\tau=t}^T \gamma^{\tau-t} r_\tau$, representing the discounted cumulative reward from t until the terminal time T . Offline RL is particularly beneficial when real-time exploration is costly or impractical, while sufficient historical data are available.

3.2 The EV Smart Charging Problem

Working closely with a charge point operator (CPO), it was evident that existing heuristic and mathematical programming charging strategies don't scale efficiently as EV fleets grow. To address this, we designed the state-action space and objectives around real-world operational constraints and assumptions provided by the CPO. We consider a set of \mathcal{I} charging stations indexed i , all assumed to be controlled by a CPO over a time window \mathcal{T} , divided into T non-overlapping intervals. For a given time window, each charging station i operates a set of \mathcal{J} non-overlapping charging sessions, denoted by $\mathcal{J}_i = \{j_{1,i}, \dots, j_{J_i,i}\}$, where $j_{j,i}$ represents the j^{th} charging event at the i^{th} charging station and $J_i = |\mathcal{J}_i|$ is the total number of charging sessions seen by charging station i in an episode. A charging session is then represented as $j_{j,i} : \{t_{j,i}^a, t_{j,i}^d, \bar{p}_{j,i}, e_{j,i}^*\}$, $\forall j, i$, where t^a, t^d, \bar{p} and e^* represent the arrival time, departure time, maximum charging power, and the desired battery energy level at the departure time. The primary goal is to minimize the total energy cost given by:

$$f_1(p^+, p^-) = \sum_{t \in \mathcal{T}} \sum_{i \in \mathcal{I}} \Delta t (\Pi_t^+ p_{i,t}^+ - \Pi_t^- p_{i,t}^-) \quad (1)$$

$p_{i,t}^+$ and $p_{i,t}^-$ denote the charging or discharging power of the i^{th} charging station during time interval t . Π_t^+ and Π_t^- are the charging and discharging costs, respectively. Along with minimizing the total energy costs, the CPO also wants the aggregate power of all the charging stations ($p_t^\Sigma = \sum_{i \in \mathcal{I}} p_{i,t}^+ - p_{i,t}^-$) to remain below the set power limit p_t^* . By doing so, the CPO avoids paying penalties due to overuse of network capacity. Hence, we introduce the penalty:

$$f_2(p^+, p^-) = \sum_{t \in \mathcal{T}} \max\{0, p_t^\Sigma - p_t^*\}, \quad (2)$$

Maintaining the desired battery charge at departure is crucial for EV user satisfaction. We model as:

$$f_3(p^+, p^-) = \sum_{i \in \mathcal{I}} \sum_{j \in \mathcal{J}_i} \left(\sum_{t=t_{j,i}^a}^{t_{j,i}^d} (p_{i,t}^+ - p_{i,t}^-) - e_{j,i}^* \right)^2 \quad (3)$$

Eq. (3) defines a sparse reward added at each EV departure based on its departure energy level. Building on these objectives, the overall EV charging problem is formulated as:

$$\max_{p^+, p^-} (f_1(\cdot) - 100 \cdot f_2(\cdot) - 10 \cdot f_3(\cdot)) \quad (4)$$

The multi-objective optimization function in Eq.4 integrates Eqs.1–3 using experimentally determined coefficients based on practical importance. This mixed integer programming (MIP) problem is subject to lower-level operational constraints (e.g., EV battery, power levels) as detailed in Appendix A.1.

EV Charging MDP The optimal EV charging problem can be framed as an MDP: $\mathcal{M} = (\mathcal{S}, \mathcal{A}, \mathcal{P}, R)$. At any time step t , the state $s_t \in \mathcal{S}$ is represented by a dynamic graph $\mathcal{G}_t = (\mathcal{N}_t, \mathcal{E}_t)$, where \mathcal{N}_t is the set of nodes and \mathcal{E}_t is the set of edges. The graph is dynamic since the number of nodes in the state and action graph can vary in each step, because of EVs' arrival and departures. Each node $n \in \mathcal{N}_t$ has a feature vector $\mathbf{x}_n^t \in \mathbb{R}^d$, capturing node-dependent information such as power limits and prices (see Appendix A.3 for the complete definition). This graph structure [35] efficiently models evolving relationships among EVs, chargers, and the grid infrastructure. The action space $\mathcal{a}_t \in \mathcal{A}$ is represented by a dynamic graph $\mathcal{G}_t^{\mathbf{a}} = (\mathcal{N}_t^{\mathbf{a}}, \mathcal{E}_t^{\mathbf{a}})$, where nodes $\mathcal{N}_t^{\mathbf{a}}$ correspond to the decision variables of the optimization problem (e.g., EVs). Each node $n \in \mathcal{N}_t^{\mathbf{a}}$ represents a single action

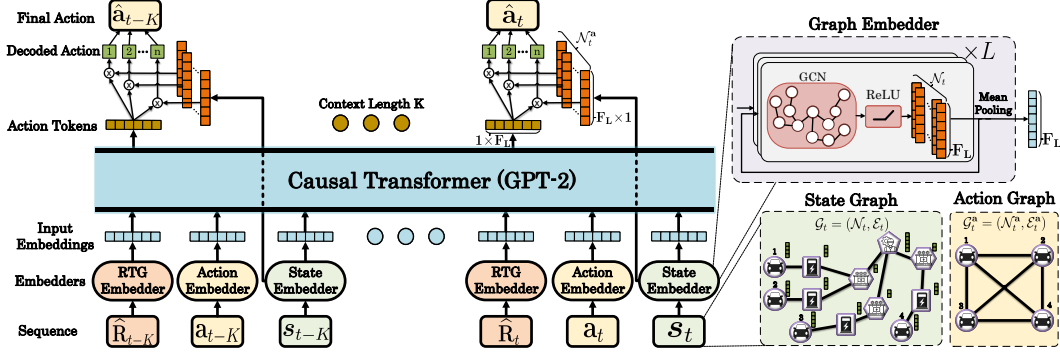


Figure 1: Overview of the GNN-DT architecture. The input sequence, comprising return-to-go, action, and state, is processed through specialized embedding modules. The action graph $\mathcal{G}_t^a = (\mathcal{N}_t^a, \mathcal{E}_t^a)$, with nodes $\mathcal{N}_t^a \subset \mathcal{N}_t$, and the state graph $\mathcal{G}_t = (\mathcal{N}_t, \mathcal{E}_t)$ are encoded using GNN-based embedders to produce embeddings of dimension F_L . These embeddings serve as inputs to a GPT-2-based causal transformer, which predicts the next action token. The predicted action token acts as a decoder, generating actions by multiplying with specific GNN state node embeddings.

$a_{i,t} \in \mathbf{a}_t$, scaled by the corresponding charger’s maximum power limit. For charging, $a_{i,t} \in [0, 1]$, and for discharging, $a_{i,t} \in [-1, 0)$. The transition function $\mathcal{P}(s_{t+1} | s_t, \mathbf{a}_t)$ accounts for uncertainties in EV arrivals, departures, energy demands, and grid fluctuations. Finally, the reward function is the same with the objective described in Eq. 4 and is defined as $R(s_t, \mathbf{a}_t) = f_1 - 100f_2 - 10f_3$ for a single timestep ($\mathcal{T} = \{t\}$). The reward is guiding the policy to maximize cost savings, respect operational constraints, and meet EV driver requirements. While Eqs.1 and 2 represent individual EV rewards and aggregated EV penalties, respectively, Eq.3 introduces a sparse reward that activates only when an EV departs, thereby creating complex temporal dependencies. The reward function weights were selected after comprehensive experimentation, ensuring the optimal solution of the MIP remains the same while the RL training is balanced between exploration and penalization.

4 GNN-based Decision Transformer

The innovative GNN-DT architecture (Fig. 1) efficiently solves optimization problems in complex environments with dynamic state-action spaces by embedding past actions, states, and returns-to-go, using a causal transformer to generate action tokens, and integrating these with current state embeddings to determine final actions within the dynamically changing action space.

4.1 Sequence Embeddings

In GNN-DT, each input “modality” is processed by a specialized embedding network. The state graph passes through the *State Embedder*, the action through the *Action Embedder*, and the return-to-go value through a simple Multi-Layer Perceptron (MLP). Compared to standard MLP embedders, GNNs provide embeddings for states and actions invariant to the number of nodes by capturing the graph structure. This design makes GNN-DT more sample-efficient during training and better at generalizing to unseen environments.

In detail, the *State Embedder* consists of L consecutive Graph Convolutional Network (GCN) [36] layers, which aggregate information from neighboring nodes as follows:

$$\mathbf{x}_t^{(l+1)} = \sigma\left(D^{-1/2} A_t D^{-1/2} \mathbf{x}_t^{(l)} W^{(l)}\right), \quad (5)$$

where $\mathbf{x}_t^{(l)} \in \mathbb{R}^{N_t \times F_l}$ denotes the node embeddings at layer l with N_t number of nodes, $W^{(l)} \in \mathbb{R}^{F_l \times F_{l+1}}$ are trainable weights, $\sigma(\cdot)$ is a nonlinear activation (ReLU), A_t is the adjacency matrix of the state graph \mathcal{G}_t , and D is the degree matrix for normalization. After the final layer, a mean-pooling operation produces a fixed-size state embedding: $\tilde{\mathbf{s}}_t = \frac{1}{|\mathcal{N}_t|} \sum_{n \in \mathcal{N}_t} \mathbf{x}_{n,t}^{(L)}$, where $\mathbf{x}_n^{(L)}$ is the embedding of node n at the L -th layer. This pooling step ensures that the state embedding is invariant to the number of nodes in the graph, enabling the architecture to scale with any number of EVs or

chargers. Similarly, the *Action Embedder* processes the action graph $\mathcal{G}_t^{\mathbf{a}} = (\mathcal{N}_t^{\mathbf{a}}, \mathcal{E}_t^{\mathbf{a}})$ through C GCN layers followed by mean pooling, producing the action embedding $\tilde{\mathbf{a}}_t$. All embedding vectors (states, actions, or the return-to-go value) have the same dimensions. This design leverages the dynamic and invariant nature of GCN-based embeddings, allowing the DT to handle variable-sized graphs.

4.2 Decoding Actions

Once the embedding sequence of length K is constructed², it is passed through the causal transformer GPT-2 to produce a fixed-size output vector $\mathbf{y}_t \in \mathbb{R}^{F_L}$ for each step. Because DT architectures inherently generate outputs of fixed dimensions, an additional mechanism is required to manage dynamic action spaces. To address this, GNN-DT implements a residual connection that merges the final GCN layer embeddings $\mathbf{x}_t^{(L)}$ with the transformer output \mathbf{y}_t for every step of the sequence. Specifically, for each node $n \in \mathcal{N}_t^{\mathbf{a}}$, we retrieve its corresponding state embedding $\mathbf{x}_{n,t}^{(L)} \in \mathbb{R}^{1 \times F_L}$ and multiply it with the transformer output token $\mathbf{y}_t \in \mathbb{R}^{1 \times F_L}$, yielding the final action for node n : $\hat{\mathbf{a}}_{n,t} = \mathbf{y}_t^{\top} \cdot \mathbf{x}_{n,t}^{(L)}$. By repeating for every step t and every node $n \in \mathcal{N}_t^{\mathbf{a}}$ the final action vector $\hat{\mathbf{a}}_t$ is generated. This design allows the model to maintain a fixed-size output from the DT while dynamically adapting to any number of nodes (and hence actions). It effectively combines the high-level context learned by the transformer with the node-specific state information captured by the GNN, enabling robust, scalable decision-making even as the graph structure changes.

4.3 Training: Action Masking and Loss Function

The proposed GNN-DT model is trained via supervised learning using an offline trajectory dataset [13], similarly to offline RL. Specifically, the GPT-2 model is initialized with its default pre-trained weights, which are subsequently fine-tuned end-to-end for the EV charging optimization task. In GNN-DT, the learning of infeasible actions, such as charging an unavailable EV, is avoided through action masking. At each time step t , a mask vector \mathbf{m}_t , which has the same dimension as \mathbf{a}_t , is generated with zeros marking invalid actions and ones marking valid actions. For example, an action is invalid when the $a_{i,t} \neq 0$ and no EV is connected at charger i . The mean squared error between the predicted actions $\hat{\mathbf{a}}_t$ and ground-truth actions \mathbf{a}_t from expert or offline trajectories is employed as the loss function. For a window of length K ending at time t , training loss is defined as:

$$\mathcal{L} = \frac{1}{K} \sum_{\tau=t-K}^t \|(\hat{\mathbf{a}}_{\tau} - \mathbf{a}_{\tau}) \circ \mathbf{m}_{\tau}\|^2. \quad (6)$$

By incorporating the mask into the loss calculation (elementwise multiplication), a focus solely on valid actions is enforced, thereby preserving meaningful gradient updates.

5 Experiments

In this section, a comprehensive set of experiments is presented to evaluate the proposed method’s performance, both during training and under varied test conditions. Different dataset types and sample sizes are examined to determine their impact on learning efficiency and convergence.

Experimental Setup The dataset generation and the evaluation experiments are conducted using the EV2Gym simulator [17], which leverages real-world data distributions, including EV arrivals, EV specifications, electricity prices, etc. This setup ensures a realistic environment where the state and action spaces accurately reflect real charging stations’ operational complexity. A scenario with 25 chargers is chosen, allowing up to 25 EVs to be connected simultaneously. In this configuration, the action vector has up to 25 variables (one per EV), while the state vector contains around 150 variables describing EV statuses, charger conditions, power transformer constraints, and broader environmental factors. Consequently, the resulting optimization problem is in the moderate-to-large scale range, reflecting the key complexities of real-world EV charging. Each training procedure is repeated 10 times with distinct random seeds to ensure statistically robust findings. All reported rewards represent the average performance over 50 evaluation scenarios, each featuring different configurations (electricity prices, EV behavior, power limits, etc.). Training was carried out on an

²During inference the action (\mathbf{a}_t) and RTG ($\hat{\mathbf{R}}_t$) of the last step t are filled with zeros as they are not known.

NVIDIA A10 GPU paired with 11 CPU cores and 80 GB of RAM, using the AdamW optimizer and a LambdaLR scheduler. Baseline RL agents converged in 2–5 hours, while the proposed GNN-DT required up to 24 hours of training. Default hyperparameters were used for all baseline RL methods; Appendix B.1 lists the full set of hyperparameters employed to train the DTs.

Dataset Generation Offline RL algorithms, including DTs, can learn policies from trajectories without needing online interaction with the environment. Consequently, the quality of the gathered training trajectories has a substantial impact on the learning process. In this work, three distinct strategies were used to generate trajectories: a) *Random*: Uniformly sampled actions in the range $[-1, 1]$ were applied to the simulator. b) *Business-as-Usual (BaU)*: A Round Robin heuristic charging policy commonly employed by CPOs, which sequentially allocates charging power among EVs to balance fairness and efficiency. c) *Optimal*: Expert solutions derived from solving offline the MIP as described in Section 3.2 for multiple scenarios. Each trajectory consists of 300 state-action-reward-action mask tuples, with each timestep representing a 15-minute interval, resulting in a total of three simulated days. This combination of random, typical, and expert data provides a comprehensive basis for evaluating how GNN-DT learns from diverse offline trajectories.

5.1 Training Performance

Fig. 2 compares the proposed GNN-DT against multiple baselines, including the classic DT [13] and Q-DT [15], which both rely on flattened state representations due to their inability to directly process graph-structured data. In these baseline methods, empty chargers and unavailable actions are replaced by zeros, so the action vector is always the same size. Several well-known online RL algorithms from the Stable-Baselines-3 [37] framework (SAC, DDPG, TD3, TRPO, PPO, and TQC) and offline RL algorithms from D3RLPY [38] (IQL, CQL, and BC) are also included. The offline RL algorithms (IQL, CQL, BC, DT, Q-DT, and GNN-DT) are trained on three datasets (*Optimal*, *Random*, and *BaU*), each comprising 10,000 trajectories. A red dotted line marks the optimal reward, which represents the experimental maximum achievable reward obtained by solving the deterministic MIP knowing the future (*Oracle*) defined in Appendix A.1. This oracle reward serves as an upper bound and helps contextualize the relative performance of each method. It is important to note that the EV smart charging problem requires real-time (1-5 min intervals) optimization solutions for large-scale, highly stochastic scenarios, where metaheuristic algorithms, stochastic optimization, and model predictive control methods fail due to computational constraints. By contrast, once trained (over 2–24 hours), RL agents can deliver real-time charging schedules on an ordinary computer in milliseconds.

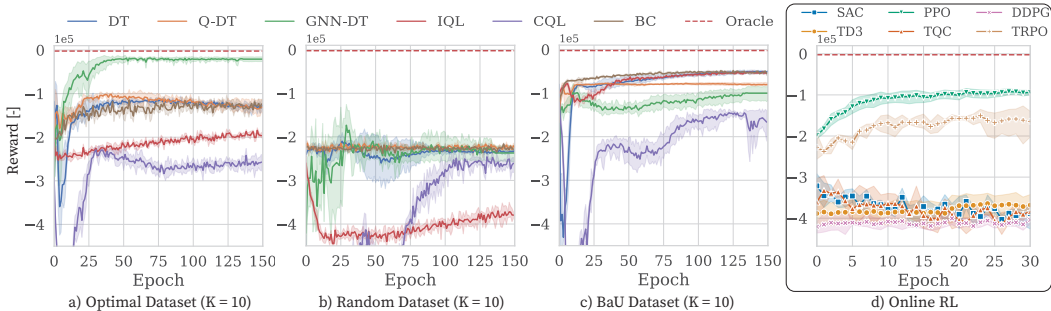


Figure 2: Training performance comparison for online and offline RL algorithms.

In Figs. 2.a-c, the DT-based approaches use a context length $K = 10$. As expected, the *Optimal* dataset provides the highest-quality information, enabling GNN-DT to converge rapidly toward near-oracle performance, while classic DT, Q-DT, and the other offline RL algorithms lag far behind, showcasing GNN-DT’s improved sample efficiency. With the *Random* dataset, the limited quality of data leads all methods to plateau at lower reward values, although GNN-DT still surpasses the other baselines. An intriguing behavior is observed with the *BaU* dataset, where classic DT, BC, and IQL converge at rewards exceeding that of GNN-DT. In contrast, the online RL algorithms displayed in Fig. 2.d struggle to achieve comparable improvements, suggesting that pure online exploration is insufficient for solving this complex EV charging optimization problem with sparse rewards. For completeness, Appendices B.2 and B.3 contain the training curves for all algorithm-dataset-context

Table 1: Comparison of maximum episode rewards ($\times 10^5$) for baselines and GNN-DT across datasets and context lengths (K). **Bold** indicates the highest value within each dataset and K category.

Dataset	Avg. Training Dataset Reward	K=2			K=10		
		DT	Q-DT	GNN-DT	DT	Q-DT	GNN-DT
Random 100		-1.91	-1.97	-0.82	-2.12	-2.09	-1.16
Random 1000	-2.37 \pm 0.39	-1.93	-2.04	-0.86	-2.11	-2.01	-1.18
Random 10000		-1.76	-2.04	-1.25	-1.81	-1.98	-0.98
BaU 100		-0.79	-0.74	-0.59	-0.79	-0.72	-0.56
BaU 1000	-0.67 \pm 0.07	-0.71	-0.66	-0.65	-0.64	-0.71	-0.57
BaU 10000		-0.69	-0.66	-0.66	-0.44	-0.74	-0.53
Optimal 100		-0.67	-0.91	-0.15	-1.12	-0.90	-0.14
Optimal 1000	-0.01 \pm 0.01	-0.63	-0.67	-0.10	-0.87	-0.86	-0.09
Optimal 10000		-0.63	-0.80	-0.04	-0.72	-0.90	-0.07

length configurations used. In the rest of this section, we omit the online and offline RL baselines, as their performance is substantially inferior to that of DT, Q-DT, and GNN-DT.

Dataset Impact In Table 1, the maximum episode reward is compared for small, medium, and large datasets (100, 1,000, and 10,000 trajectories), under two different context lengths ($K = 2$ and $K = 10$). The left side of Table 1 reports the dataset type, the number of trajectories, and the average reward in each dataset. All baselines achieve performance above the *Random* dataset’s average reward. However, only GNN-DT consistently approaches the *Optimal* dataset’s performance, reaching as close as -0.04×10^5 compared to the -0.01×10^5 optimal reward. This advantage becomes especially evident at the largest dataset size (10,000 trajectories), highlighting the benefits of the graph-based embedding layer. Overall, GNN-DT outperforms the baselines across all datasets and both context lengths, with the single exception of the *BaU* dataset at $K = 10$. Interestingly, a larger context window does not always translate into higher rewards, potentially due to the problem setting. Similarly, the dataset size appears to have minimal impact on Q-DT, whereas DT and GNN-DT generally improve with more trajectories. These findings underscore that both the quality and quantity of offline data, coupled with the GNN-DT architecture, are key to achieving superior performance.

Enhancing Training Datasets The previous section highlighted that the quality of trajectories in the training dataset is the most influential factor for achieving high performance. In this section, we explore whether creating new datasets by mixing existing ones can further improve performance. The *Optimal* and *Random* datasets are combined in different proportions, as summarized in Table 2. A noteworthy result is that supplementing the *Optimal* dataset with theoretically less useful (*Random*) trajectories consistently boosts performance. In particular, GNN-DT with $K = 10$, trained on a mix of 250 *Optimal* and 750 *Random* trajectories, achieves near-oracle results, deviating by only -0.001×10^5 from the optimal reward. A similar trend emerges when blending *BaU* and *Random* datasets (Table 8 in Appendix B.4), although the performance gains are not as significant. Overall, these findings indicate that carefully integrating high- and lower-quality data can enhance policy learning beyond what purely *Optimal* or purely *Random* datasets can provide.

Table 2: Maximum reward of GNN-DT trained on merged *Optimal* and *Random* datasets for $K = 2$ and $K = 10$. Highest rewards per K are highlighted with **bold**.

Dataset	Total Traj.	Avg. Dataset Reward	GNN-DT Reward ($\times 10^5$)	
			K=2	K=10
Random (Rnd.) 100%	1000	-2.37 \pm 0.39	-0.863	-1.187
Opt. 25% + Rnd. 75%	1000	-1.78 \pm 1.07	-0.045	-0.020
Opt. 50% + Rnd. 50%	1000	-1.18 \pm 1.19	-0.021	-0.040
Opt. 75% + Rnd. 25%	1000	-0.60 \pm 1.03	-0.073	-0.057
Optimal (Opt.) 100%	1000	-0.01 \pm 0.01	-0.108	-0.099

Component Ablation Study To better understand the contribution of each architectural component, we conduct an ablation study that systematically removes or replaces elements of our model and then

Table 3: Average reward trained over 5 runs with different seeds for *Optimal* and *Mixed* datasets.

DT	State GNN	Action GNN	Res. Con.	Action Mask	Optimal ($\times 10^5$)	Mixed ($\times 10^5$)
✓	✗	✗	✗	✗	-0.69 ± 0.03	-0.95 ± 0.39
✓	GCN	✗	✗	✗	-0.71 ± 0.02	-0.77 ± 0.17
✓	GCN	✗	✓	✗	-0.18 ± 0.03	-0.16 ± 0.07
✓	GCN	GCN	✓	✗	-0.11 ± 0.03	-0.12 ± 0.04
✓	GAT	GAT	✓	✓	-0.14 ± 0.07	-0.15 ± 0.06
✓	GCN	GCN	✓	✓	-0.09 ± 0.02	-0.10 ± 0.04

trains the model on the *Optimal* and *Mixed* (Opt.25%+Rand.75%). The results in Table 3 reveal that neither a plain DT nor a DT augmented solely with a state-GNN submodule achieves competitive performance. Notably, adding the residual connection atop the state-GNN leads to a significant improvement, from -0.77×10^5 to -0.16×10^5 on the *Mixed* dataset, demonstrating its importance for effective credit assignment over dynamic inputs. Removing action masking or replacing the GCN module with a Graph Attention Network (GAT) [39] similarly degrades performance, indicating that each component provides distinct and complementary benefits. Ultimately, only the full GNN-DT architecture achieves strong performance across both the *Mixed* and *Optimal* datasets.

5.2 Illustrative Example of EV Charging

With the models trained, we proceed to compare the behavior of the best baseline models trained (DT, Q-DT, GNN-DT) against the heuristic BaU algorithm in an EV charging scenario. Fig. 3a presents the SoC progress for three EVs connected one after the other to a single charger throughout the simulation, while Fig. 3b shows the actions of all chargers taken by each algorithm.

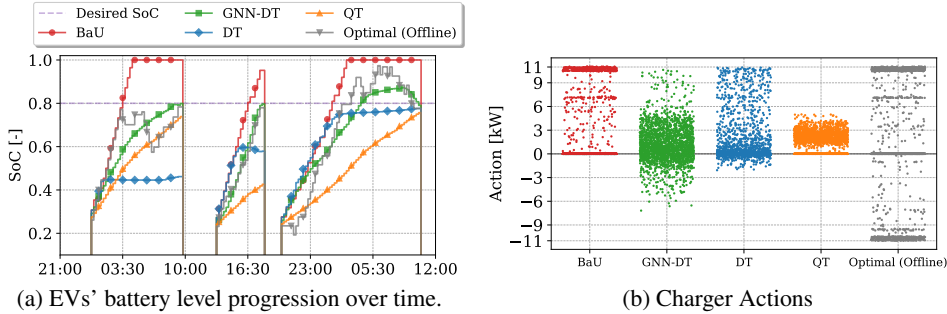


Figure 3: Comparison of smart charging algorithms for a single simulation day.

In Fig. 3a, the heuristic BaU algorithm consistently overcharges the EVs, often exceeding the desired SoC levels. In contrast, both DT and Q-DT fail to satisfy the desired SoC. Conversely, GNN-DT successfully achieves the desired SoC for all EVs, closely mirroring the behavior of the optimal algorithm. This demonstrates GNN-DT’s ability to precisely control charging based on dynamic state information. Fig. 3b provides further insights into the actions taken by each algorithm. The optimal solution primarily employs maximum charging or discharging power, since it knows the future. In comparison, GNN-DT exhibits a more refined approach, modulating charging power within a range of -6 to 11 kW. Baseline DT and Q-DT display a narrower range of actions, limiting their ability to optimize the charging schedules and adapt to varying conditions. These results underscore the superior capability of GNN-DT in managing the complexities of EV charging dynamics. For a more detailed analysis of key performance metrics in EV charging scenarios, refer to Appendix A.4.

5.3 Evaluation of Generalization and Scalability

Generalization Analysis Evaluating the generalization of RL models across varying state transition probabilities is crucial for ensuring consistent performance under diverse conditions [40]. In Fig. 4a, the generalization capabilities of GNN-DT and other baselines are assessed in environments with small, medium, and extreme variations in state transition probabilities (compared to the training environment, see Appendix A.5 for more details about the different distributions). While the baseline methods experience significant performance drops as the evaluation environment deviates from the

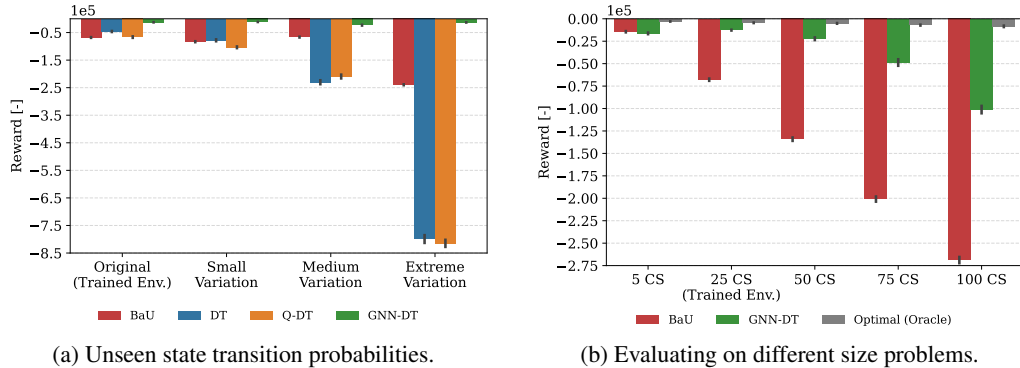


Figure 4: Generalization performance of the proposed model, depicting the average rewards achieved across 100 randomly generated scenarios in previously unseen environments.

training setting, GNN-DT maintains strong performance across all scenarios. This highlights the critical role of GNN-based embeddings in improving model robustness and generalization. A key advantage of the GNN-DT architecture, not present in classic DTs, is its invariance to problem size, i.e., the same RL agent can be applied to both smaller and larger-scale environments. Fig. 4b illustrates the scalability and generalization performance of GNN-DT compared to the BaU algorithm and Optimal policy. GNN-DT, trained on a 25-charger setup, was tested on 5, 50, 75, and 100-charger environments. While its performance predictably declines at larger scales, since it wasn’t trained on them, it still outperforms the BaU heuristic, demonstrating robustness to problem-size variation. Training GNN-DT on a mix of charger numbers could potentially further improve its adaptability.

Scalability Analysis The scalability and effectiveness of GNN-DT were tested when trained on a significantly larger optimization problem involving 250 charging stations. In this scenario, the model must handle up to 250 action variables per step and over 1,000 state variables, which include critical information such as power limits and battery levels. The results presented in Table 4 demonstrate that GNN-DT shows promise for addressing more complex optimization tasks. However, the model requires a substantial increase in both the number of training trajectories and memory resources to maintain efficiency, highlighting a well-known limitation of DT-based approaches. Scaling the problem 10× roughly multiplies GPU memory usage, e.g. storing 3,000 trajectories takes ≈ 2 GB for 25 chargers versus ≈ 20 GB for 250. While this can bottleneck large-scale training, parallelization and mini-batching mitigate it, and overall compute scales with the transformer’s context length K (see Fig. 8), pointing to interesting directions for very large problem graphs as future work.

Table 4: Max. reward of GNN-DT in a large-scale EV charging optimization task with 250 chargers.

	Total Trajectories	Avg. Dataset Reward	GNN-DT Reward
Random	3000	-22.39 ± 1.49	-9.34
BaU	3000	-6.67 ± 0.32	-4.23
Optimal	3000	-0.08 ± 0.03	-0.27

6 Conclusions

In this work, we introduced a novel DT-based architecture, GNN-DT, which incorporates GNN embedders to significantly enhance sample efficiency and overall performance in the sequential decision-making problem of EV charging. Through extensive evaluation across various datasets, including optimal, random, and BaU, we demonstrated that traditional DTs, online and offline RL algorithms fail to effectively solve real-world problems without specialized embeddings. We further show that both the size and quality of input trajectories critically impact the training process, underscoring the importance of carefully selecting datasets for effective learning. Finally, by leveraging the power of GNN embeddings, GNN-DT improved the model’s ability to generalize in previously unseen environments and handle large, complex action spaces. These contributions demonstrate GNN-DT’s potential to address complex dynamic optimization challenges beyond EV charging.

References

- [1] Line A. Roald, David Pozo, Anthony Papavasiliou, Daniel K. Molzahn, Jalal Kazempour, and Antonio Conejo. Power systems optimization under uncertainty: A review of methods and applications. *Electric Power Systems Research*, 214:108725, 2023. ISSN 0378-7796. doi: <https://doi.org/10.1016/j.epsr.2022.108725>. URL <https://www.sciencedirect.com/science/article/pii/S0378779622007842>.
- [2] Grigorios D. Konstantakopoulos, Sotiris P. Gayialis, and Evripidis P. Kechagias. Vehicle routing problem and related algorithms for logistics distribution: a literature review and classification. *Operational Research*, 22(3):2033–2062, July 2022. ISSN 1866-1505. doi: [10.1007/s12351-020-00600-7](https://doi.org/10.1007/s12351-020-00600-7). URL <https://doi.org/10.1007/s12351-020-00600-7>.
- [3] Abhishek Gunjan and Siddhartha Bhattacharyya. A brief review of portfolio optimization techniques. *Artificial Intelligence Review*, 56(5):3847–3886, 2023.
- [4] Kapil Gupta and Munish Kumar Gupta, editors. *Optimization of Manufacturing Processes*. Springer Series in Advanced Manufacturing, 2020.
- [5] Nanda Kishor Panda and Simon H. Tindemans. Quantifying the aggregate flexibility of ev charging stations for dependable congestion management products: A dutch case study, 2024.
- [6] Sébastien Bubeck. *Convex Optimization: Algorithms and Complexity*. Now Foundations and Trends, 2015. doi: [10.1561/22000000050](https://doi.org/10.1561/22000000050).
- [7] Richard S Sutton and Andrew G Barto. *Reinforcement learning: An introduction*. MIT press, 2018.
- [8] Qingfeng Lan, A. Rupam Mahmood, Shuicheng Yan, and Zhongwen Xu. Learning to optimize for reinforcement learning, 2023.
- [9] Jiayi Zhang, Chang Liu, Xijun Li, Hui-Ling Zhen, Mingxuan Yuan, Yawen Li, and Junchi Yan. A survey for solving mixed integer programming via machine learning. *Neurocomputing*, 519: 205–217, 2023. ISSN 0925-2312. doi: <https://doi.org/10.1016/j.neucom.2022.11.024>. URL <https://www.sciencedirect.com/science/article/pii/S0925231222014035>.
- [10] Sebastian Jaimungal. Reinforcement learning and stochastic optimisation. *Finance and Stochastics*, 26(1):103–129, January 2022. ISSN 1432-1122. doi: [10.1007/s00780-021-00467-2](https://doi.org/10.1007/s00780-021-00467-2). URL <https://doi.org/10.1007/s00780-021-00467-2>.
- [11] Gabriel Dulac-Arnold, Nir Levine, Daniel J. Mankowitz, Jerry Li, Cosmin Paduraru, Sven Gowal, and Todd Hester. Challenges of real-world reinforcement learning: definitions, benchmarks and analysis. *Machine Learning*, 110(9):2419–2468, September 2021. ISSN 1573-0565. doi: [10.1007/s10994-021-05961-4](https://doi.org/10.1007/s10994-021-05961-4). URL <https://doi.org/10.1007/s10994-021-05961-4>.
- [12] Bin Wang. Domain Adaptation in Reinforcement Learning: Approaches, Limitations, and Future Directions. *Journal of The Institution of Engineers (India): Series B*, 105(5):1223–1240, October 2024. ISSN 2250-2114. doi: [10.1007/s40031-024-01049-4](https://doi.org/10.1007/s40031-024-01049-4). URL <https://doi.org/10.1007/s40031-024-01049-4>.
- [13] Lili Chen, Kevin Lu, Aravind Rajeswaran, Kimin Lee, Aditya Grover, Michael Laskin, Pieter Abbeel, Aravind Srinivas, and Igor Mordatch. Decision transformer: Reinforcement learning via sequence modeling, 2021.
- [14] Zhiyue Zhang, Hongyuan Mei, and Yanxun Xu. Continuous-time decision transformer for healthcare applications. *Proceedings of Machine Learning Research*, 206:6245–6262, April 2023.
- [15] Shengchao Hu, Ziqing Fan, Chaoqin Huang, Li Shen, Ya Zhang, Yanfeng Wang, and Dacheng Tao. Q-value regularized transformer for offline reinforcement learning. In *Forty-first International Conference on Machine Learning*, 2024. URL <https://openreview.net/forum?id=ojtddicekd>.

- [16] Keiran Paster, Sheila A. McIlraith, and Jimmy Ba. You can't count on luck: why decision transformers and rvs fail in stochastic environments. In *Proceedings of the 36th International Conference on Neural Information Processing Systems*, NIPS '22, Red Hook, NY, USA, 2024. Curran Associates Inc. ISBN 9781713871088.
- [17] Stavros Orfanoudakis, Cesar Diaz-Londono, Yunus Emre Yilmaz, Peter Palensky, and Pedro P. Vergara. Ev2gym: A flexible v2g simulator for ev smart charging research and benchmarking. *IEEE Transactions on Intelligent Transportation Systems*, pages 1–12, 2024. doi: 10.1109/TITS.2024.3510945.
- [18] Yueh-Hua Wu, Xiaolong Wang, and Masashi Hamaya. Elastic decision transformer. In *Proceedings of the 37th International Conference on Neural Information Processing Systems*, NIPS '23, Red Hook, NY, USA, 2024. Curran Associates Inc.
- [19] Kuang-Huei Lee, Ofir Nachum, Mengjiao Yang, Lisa Lee, Daniel Freeman, Winnie Xu, Sergio Guadarrama, Ian Fischer, Eric Jang, Henryk Michalewski, and Igor Mordatch. Multi-game decision transformers. In *Proceedings of the 36th International Conference on Neural Information Processing Systems*, NIPS '22, Red Hook, NY, USA, 2024. Curran Associates Inc. ISBN 9781713871088.
- [20] Qinqing Zheng, Amy Zhang, and Aditya Grover. Online decision transformer. In Kamalika Chaudhuri, Stefanie Jegelka, Le Song, Csaba Szepesvari, Gang Niu, and Sivan Sabato, editors, *Proceedings of the 39th International Conference on Machine Learning*, volume 162 of *Proceedings of Machine Learning Research*, pages 27042–27059. PMLR, 17–23 Jul 2022. URL <https://proceedings.mlr.press/v162/zheng22c.html>.
- [21] Enrique Adrian Villarrubia-Martin, Luis Rodriguez-Benitez, Luis Jimenez-Linares, David Muñoz-Valero, and Jun Liu. A hybrid online off-policy reinforcement learning agent framework supported by transformers. *International Journal of Neural Systems*, 33(12), October 2023. ISSN 0129-0657. doi: 10.1142/s012906572350065x.
- [22] Zuxin Liu, Zijian Guo, Yihang Yao, Zhepeng Cen, Wenhao Yu, Tingnan Zhang, and Ding Zhao. Constrained decision transformer for offline safe reinforcement learning, 2023.
- [23] Kihyuk Hong, Yuhang Li, and Ambuj Tewari. A primal-dual-critic algorithm for offline constrained reinforcement learning. In Sanjoy Dasgupta, Stephan Mandt, and Yingzhen Li, editors, *Proceedings of The 27th International Conference on Artificial Intelligence and Statistics*, volume 238 of *Proceedings of Machine Learning Research*, pages 280–288. PMLR, 02–04 May 2024. URL <https://proceedings.mlr.press/v238/hong24a.html>.
- [24] Yao Lai, Jinxin Liu, Zhentao Tang, Bin Wang, Jianye Hao, and Ping Luo. ChiPFormer: Transferable chip placement via offline decision transformer. In Andreas Krause, Emma Brunskill, Kyunghyun Cho, Barbara Engelhardt, Sivan Sabato, and Jonathan Scarlett, editors, *Proceedings of the 40th International Conference on Machine Learning*, volume 202 of *Proceedings of Machine Learning Research*, pages 18346–18364. PMLR, 23–29 Jul 2023. URL <https://proceedings.mlr.press/v202/lai23c.html>.
- [25] Dawei Qiu, Yi Wang, Weiqi Hua, and Goran Strbac. Reinforcement learning for electric vehicle applications in power systems: a critical review. *Renewable and Sustainable Energy Reviews*, 173:113052, 2023. ISSN 1364-0321. doi: <https://doi.org/10.1016/j.rser.2022.113052>. URL <https://www.sciencedirect.com/science/article/pii/S1364032122009339>.
- [26] Ruiyang Jin, Yuke Zhou, Chao Lu, and Jie Song. Deep reinforcement learning-based strategy for charging station participating in demand response. *Applied Energy*, 328:120140, 2022. ISSN 0306-2619. doi: <https://doi.org/10.1016/j.apenergy.2022.120140>. URL <https://www.sciencedirect.com/science/article/pii/S0306261922013976>.
- [27] Jiangliang Jin and Yunjian Xu. Optimal policy characterization enhanced actor-critic approach for electric vehicle charging scheduling in a power distribution network. *IEEE Transactions on Smart Grid*, 12(2):1416–1428, 2021. doi: 10.1109/TSG.2020.3028470.
- [28] Nasrin Sadeghianpourhamami, Johannes Deleu, and Chris Develder. Definition and evaluation of model-free coordination of electrical vehicle charging with reinforcement learning. *IEEE Transactions on Smart Grid*, 11(1):203–214, 2020. doi: 10.1109/TSG.2019.2920320.

- [29] Yunus Emre Yılmaz, Stavros Orfanoudakis, and Pedro P. Vergara. Reinforcement learning for optimized ev charging through power setpoint tracking. In *2024 IEEE PES Innovative Smart Grid Technologies Europe (ISGT EUROPE)*, pages 1–5, 2024.
- [30] Sichen Li, Weihao Hu, Di Cao, Tomislav Dragičević, Qi Huang, Zhe Chen, and Frede Blaabjerg. Electric vehicle charging management based on deep reinforcement learning. *Journal of Modern Power Systems and Clean Energy*, 10(3):719–730, 2022. doi: 10.35833/MPCE.2020.000460.
- [31] Shulei Zhang, Runda Jia, Hengxin Pan, and Yankai Cao. A safe reinforcement learning-based charging strategy for electric vehicles in residential microgrid. *Applied Energy*, 348: 121490, 2023. ISSN 0306-2619. doi: <https://doi.org/10.1016/j.apenergy.2023.121490>. URL <https://www.sciencedirect.com/science/article/pii/S0306261923008541>.
- [32] Guibin. Chen and Xiaoying. Shi. A deep reinforcement learning-based charging scheduling approach with augmented lagrangian for electric vehicle, 2022.
- [33] Arian Shah Kamrani, Anoosh Dini, Hanane Dagdougui, and Keyhan Sheshyekani. Multi-agent deep reinforcement learning with online and fair optimal dispatch of ev aggregators. *Machine Learning with Applications*, page 100620, 2025. ISSN 2666-8270. doi: <https://doi.org/10.1016/j.mlwa.2025.100620>. URL <https://www.sciencedirect.com/science/article/pii/S2666827025000039>.
- [34] Sergey Levine, Aviral Kumar, George Tucker, and Justin Fu. Offline reinforcement learning: Tutorial, review, and perspectives on open problems, 2020.
- [35] Stavros Orfanoudakis, Valentin Robu, Edgar Mauricio Salazar Duque, et al. Scalable reinforcement learning for large-scale coordination of electric vehicles using graph neural networks. Preprint (Version 1) available at Research Square, December 2024. URL <https://doi.org/10.21203/rs.3.rs-5504138/v1>. Accessed on 19 December 2024.
- [36] Thomas N. Kipf and Max Welling. Semi-supervised classification with graph convolutional networks, 2016.
- [37] Antonin Raffin, Ashley Hill, Adam Gleave, Anssi Kanervisto, Maximilian Ernestus, and Noah Dormann. Stable-baselines3: Reliable reinforcement learning implementations. *Journal of Machine Learning Research*, 22(268):1–8, 2021. URL <http://jmlr.org/papers/v22/20-1364.html>.
- [38] Takuma Seno and Michita Imai. d3rlpy: An offline deep reinforcement learning library. *Journal of Machine Learning Research*, 23(315):1–20, 2022. URL <http://jmlr.org/papers/v23/22-0017.html>.
- [39] Petar Veličković, Guillem Cucurull, Arantxa Casanova, Adriana Romero, Pietro Liò, and Yoshua Bengio. Graph attention networks, 2018. URL <https://arxiv.org/abs/1710.10903>.
- [40] Ruosong Wang, Dean P. Foster, and Sham M. Kakade. What are the statistical limits of offline rl with linear function approximation?, 2020.

A Appendix: EV Charging Model

The first appendix Section provides the complete mixed integer programming (MIP) and MDP formulation of the optimal EV charging problem and presents detailed experimental results for key evaluation metrics.

A.1 Complete EV charging MIP model

The optimal EV charging problem we investigate aims to maximize the CPO's profits while ensuring that the demands of EV users are fully satisfied. The CPO lacks prior knowledge of when EVs will arrive or the aggregated power constraints. However, it is assumed that when an EV arrives at charging station i initiating charging session j , it provides its departure time ($t_{j,i}^d$) and the desired battery capacity ($e_{j,i}^*$) at departure. Additionally, the battery capacity $e_{i,t}$ for each EV is known while it is connected to the charger. These assumptions are standard in research, as this information can typically be retrieved through evolving charging communication protocols.

The investigated EV charging problem (See notation Table 5) expands over a simulation with t timesteps, $t \in \mathcal{T}$ where a CPO decides the charging and discharging power ($p_{i,t}^+$ and $p_{i,t}^-$) for every charging station $i \in \mathcal{I}$. Since the chargers can be spread around the city, there are charger groups $w \in \mathcal{W}$, that can have a lower-level aggregated power limits representing connections to local power

Table 5: Notation for the EV Charging Optimization Problem

Symbol	Name	Description
<i>Sets</i>		
\mathcal{T}	Set of timesteps	Time horizon for optimization
\mathcal{I}	Set of charging stations	All EV charging stations
\mathcal{W}	Set of charger groups	Chargers grouped by local transformer connections
\mathcal{J}_i	Set of charging sessions	Charging sessions at charger i
<i>Indexes</i>		
t	Timestep index	Discrete time step
i	Charger index	Individual EV charging station
j	Session index	Charging session at a charger
w	Charger group index	Charger groups connected to transformers
<i>Parameters</i>		
$t_{j,i}^a$	Arrival time	Time EV j arrives at charger i
$t_{j,i}^d$	Departure time	Time EV j departs charger i
$e_{j,i}^*$	Desired battery capacity	Desired battery energy at departure for session j at charger i
$e_{j,i}^a$	Arrival battery energy	Battery energy at EV arrival
$\underline{e}_{j,i}, \bar{e}_{j,i}$	Battery limits	Min/max allowable battery energy
$\underline{p}_{j,i}^+, \bar{p}_{j,i}^+$	Charging power limits	Min/max charging power
$\underline{p}_{j,i}^-, \bar{p}_{j,i}^-$	Discharging power limits	Min/max discharging power
p_t^*	Total power limit	Desired aggregated power
Π_t^+, Π_t^-	Electricity prices	Prices for charging/discharging at timestep t
Δt	Time interval	Duration of each timestep
$\bar{p}_{w,t}$	Group power limit	Power limit for group w at timestep t
<i>Variables</i>		
$p_{i,t}^+, p_{i,t}^-$	Charging/discharging power	Power assigned at charger i , timestep t
$\omega_{i,t}^+, \omega_{i,t}^-$	Binary operation indicators	Indicates if charger i charges (+) or discharges (-) at timestep t
$e_{j,i,t}$	EV battery energy	Battery level for session j at charger i , timestep t
p_t^-	Total aggregated power	Net total power across all chargers at timestep t

transformers. Based on these factors, the overall optimization objective is defined as follows:

$$\max_{p^+, \omega^+, p^-, \omega^-} \sum_{t \in \mathcal{T}} \left(-100 \cdot \max\{0, p_t^\Sigma - p_t^*\} \right) \quad (7)$$

$$+ \sum_{i \in \mathcal{I}} \left(\Delta t \left(\Pi_t^+ p_{i,t}^+ \omega_{i,t}^+ - \Pi_t^- p_{i,t}^- \omega_{i,t}^- \right) \right) \quad (8)$$

$$- 10 \cdot \sum_{j \in \mathcal{J}_i} \left(\sum_{t=t_{j,i}^a}^{t_{j,i}^d} \left(p_{i,t}^+ \omega_{i,t}^+ - p_{i,t}^- \omega_{i,t}^- \right) - e_{j,i}^* \right)^2 \quad (9)$$

Subject to:

$$p_t^\Sigma = \sum_{i \in \mathcal{I}} p_{i,t}^+ \cdot \omega_{i,t}^+ - p_{i,t}^- \cdot \omega_{i,t}^- \quad \forall i, \forall t \quad (10)$$

$$\bar{p}_{w,t} \geq \sum_{i \in \mathcal{W}_i} p_{i,t}^+ \cdot \omega_{i,t}^+ - p_{i,t}^- \cdot \omega_{i,t}^- \quad \forall i, \forall w, \forall t \quad (11)$$

$$e_{j,i} \leq e_{j,i,t} \leq \bar{e}_{j,i} \quad \forall j, \forall i, \forall t \quad (12)$$

$$e_{j,i,t} = e_{j,i,t-1} + (p_{i,t}^+ \cdot \omega_{i,t}^+ + p_{i,t}^- \cdot \omega_{i,t}^-) \cdot \Delta t \quad \forall j, \forall i, \forall t \quad (13)$$

$$e_{j,i,t} = e_{j,i}^a \quad \forall j, \forall i, \forall t = t_{j,i}^a \quad (14)$$

$$\underline{p}_{j,i}^+ \leq p_{i,t}^+ \leq \bar{p}_{j,i}^+ \quad \forall j, \forall i, \forall t \quad (15)$$

$$\underline{p}_{j,i}^- \leq p_{i,t}^- \leq \bar{p}_{j,i}^- \quad \forall j, \forall i, \forall t \quad (16)$$

$$\omega_{i,t}^+ + \omega_{i,t}^- \leq 1 \quad \forall i, \forall t \quad (17)$$

The power of a single charger i is modeled using four decision variables, $p^+ \cdot \omega^+$ and $p^- \cdot \omega^-$, where ω^+ and ω^- are binary variables, to differentiate between charging and discharging behaviors and enable charging power to get values in ranges $0 \cup [\underline{p}^+, \bar{p}^+]$, and discharging power in $[\underline{p}^-, \bar{p}^-] \cup 0$. Eq. 11 defines the locally aggregated transformer power limits \bar{p} for chargers belonging to groups \mathcal{W}_i . Eqs.(13) and(14) address EV battery constraints during operation with a minimum and maximum capacity of \underline{e} , \bar{e} , and energy e^a at time of arrival t^a . Equations (15) and (16) impose charging and discharging power limits for every charger-EV session combination. To prevent simultaneous charging and discharging, the binary variables ω^{ch} and ω^{dis} are constrained by (17).

A.2 Evaluation Metrics

The following evaluation metrics are used in this study to assess the performance of the proposed algorithms:

User Satisfaction [%]: This metric measures how closely the state of charge (SoC) of an EV at departure matches its target SoC*. For a set of EVs \mathcal{J} , user satisfaction is given by:

$$\text{User Sat.} = \frac{1}{|\mathcal{J}|} \cdot \sum_{j \in \mathcal{J}} \left(\frac{e_{j,t^d}}{e_j^*} \right) \cdot 100\%. \quad (18)$$

This ensures that each EV is charged to its desired level by the end of the charging session.

Energy Charged [kWh]: This represents the total energy supplied to EVs over the entire charging period and is given by:

$$\text{Energy Charged} = \sum_{t \in \mathcal{T}} \sum_{i \in \mathcal{I}} p_{i,t}^+ \cdot \omega_{i,t}^+ \cdot \Delta t. \quad (19)$$

This metric helps quantify the overall energy throughput for the system.

Energy Discharged [kWh]: This measures the amount of energy discharged back to the grid by the EVs. Discharging is typically done when electricity prices are high, and this metric is important for evaluating the system's ability to contribute to grid stability.

$$\text{Energy Discharged} = \sum_{t \in \mathcal{T}} \sum_{i \in \mathcal{I}} p_{i,t}^- \cdot \omega_{i,t}^- \cdot \Delta t. \quad (20)$$

Power Violation [kW]: This metric tracks violations of operational constraints, such as exceeding the aggregated power limits at any given time. A violation occurs when the total power used exceeds the maximum allowed power:

$$\text{Power Violation} = \sum_{t \in \mathcal{T}} \max\{0, p_t^\Sigma - p_t^*\} \Delta t. \quad (21)$$

Minimizing this metric ensures that the system remains within operational limits and avoids overloading the grid.

Cost [€]: This evaluates the financial cost of the charging operations, considering both charging and discharging costs based on electricity prices. The total cost over the simulation period is defined as:

$$\text{Cost} = \sum_{t \in \mathcal{T}} \sum_{i \in \mathcal{I}} \Delta t (\Pi_t^+ p_{i,t}^+ - \Pi_t^- p_{i,t}^-), \quad (22)$$

This metric helps assess the cost-effectiveness of the charging strategy.

A.3 The MDP State Space

At each time step t , the environment state $\mathbf{s}_t \in \mathcal{S}$ is encoded as a heterogeneous graph $\mathcal{G}_t = (\mathcal{N}_t, \mathcal{E}_t)$, where \mathcal{N}_t is the set of nodes (EVs, chargers, transformer, and CPO) and \mathcal{E}_t the set of edges encoding physical and informational connections. Each node $n \in \mathcal{N}_t$ carries a feature vector $\mathbf{x}_n^t \in \mathbb{R}^d$, encapsulating all observations available to the CPO under V2G protocols. Fig. 5 shows how the EV charging problem is modelled as a graph with each node type having different number of features as detailed below.

An EV node's feature vector:

$$\mathbf{x}_t^{\text{ev}} = [\text{SoC}_t, t^{\text{d}} - t, j, i, w] \quad (23)$$

encodes its current state of charge $\text{SoC}_t \in [0, 1]$, the remaining steps until departure $t^{\text{d}} - t$, and the identifiers j, i , and w of the charging point, charger, and transformer group to which it is connected. Exact SOC and departure-time information are assumed available via ISO 15118-style V2G signaling. A charging station (cs) node i is described by:

$$\mathbf{x}_t^{\text{cs}} = [\bar{p}_{i,j}^+, \bar{p}_{i,j}^-, i], \quad (24)$$

where \bar{p}^+ and \bar{p}^- are its maximum charging and discharging power and i its unique identifier. A transformer (tr) node w has a feature vector:

$$\mathbf{x}_t^{\text{tr}} = [\bar{p}_{w,t}, w], \quad (25)$$

where $\bar{p}_{w,t}$ denotes its maximum power capacity and w its identifier, ensuring the policy respects feeder-level constraints. The CPO (system) node aggregates temporal and economic context in

$$\mathbf{x}_t^{\text{cpo}} = \left[\frac{d}{7}, \sin\left(\frac{h}{48\pi}\right), \cos\left(\frac{h}{48\pi}\right), \Pi_t^+, p_{t-1}^\Sigma \right]. \quad (26)$$

Here d and h encode day-of-week and hour to capture demand patterns, Π_t^+ is the charging price at t , and p_{t-1}^Σ is the previous time step's total power draw, providing feedback for profit-maximizing decisions.

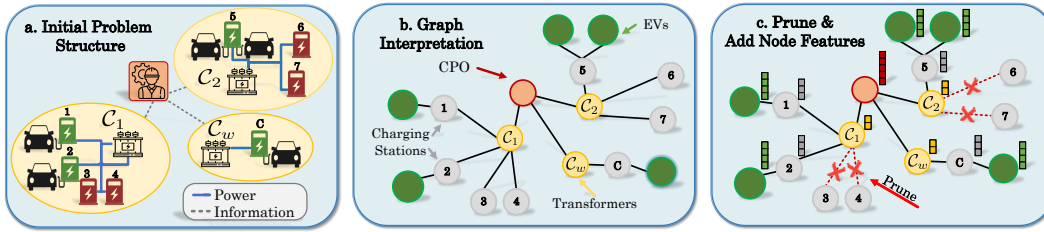


Figure 5: The EV charging problem graph structure and state. (a) shows the raw physical layout of EVs, chargers and transformer with information and power links; (b) recasts this as a four-type node graph (EV, charger, transformer, CPO) carrying only the observations available to the CPO; and (c) prunes any charger without connected EV resulting in a compact dynamic heterogeneous state graph.

A.4 Complete Experimental Results of EV Charging.

Table 6 shows a comparison of key EV charging metrics for the 25-station problem after 100 evaluations, including heuristic algorithms, Charge As Fast as Possible (CAFAP) and BaU, and DT variants with the optimal solution, which assumes future knowledge. GNN-DT shows remarkable performance, achieving a close approximation to the optimal solution, particularly in user satisfaction ($99.3\% \pm 0.03\%$) and power violation (21.7 ± 22.8 kW). It outperforms both BaU and DT variants in terms of energy discharged, power violation, and costs. Notably, GNN-DT performs well even compared to Q-DT, while maintaining competitive execution time, albeit slightly slower than the simpler models. The results underscore the effectiveness of GNN-DT in managing complex EV charging tasks, demonstrating its potential for real-world applications where future knowledge is not available.

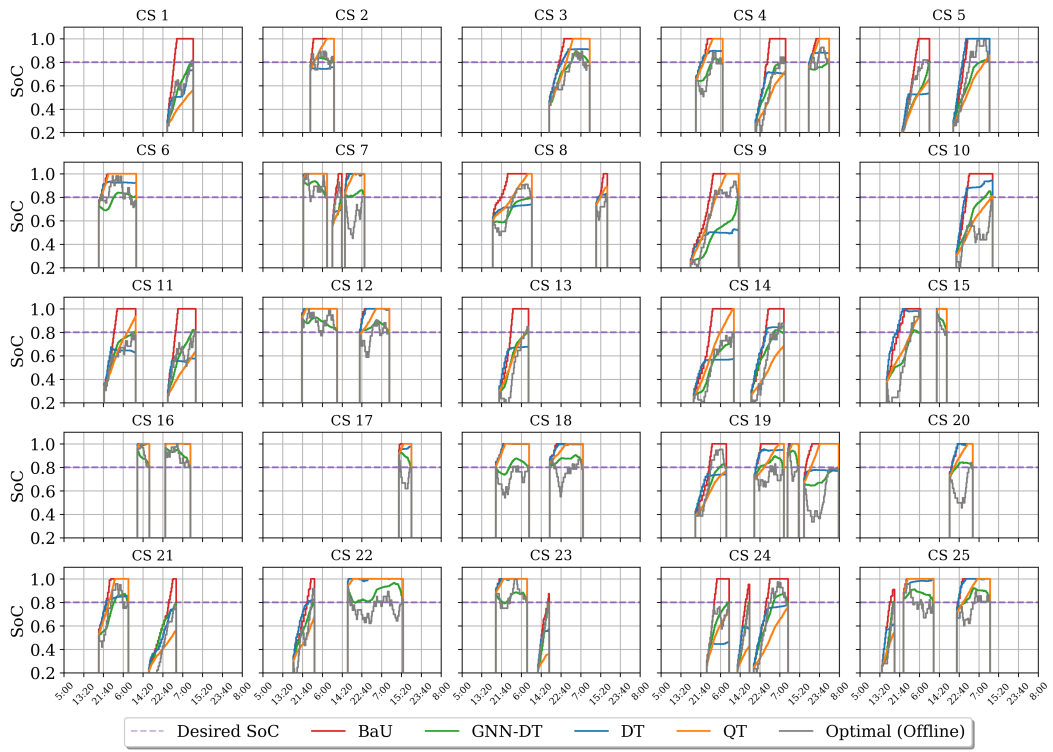
Table 6: Comparison of key EV charging metrics for the 25-station problem after 100 evaluations, for heuristic algorithms (CAFAP & BaU) and DT variants with the optimal solution, which assumes future knowledge.

Algorithm	Energy Charged [MWh]	Energy Discharged [MWh]	User Satisfaction [%]	Power Violation [kW]	Costs [€]	Reward [-10 ⁵]	Exec. Time [sec/step]
CAFAP	1.3 ±0.2	0.00 ±0.00	100.0 ±0.0	1289.2 ±261.8	-277 ±165	-1.974 ±0.283	0.001
BaU	1.3 ±0.2	0.00 ±0.00	99.9 ±0.2	10.5 ±9.4	-255 ±156	-0.679 ±0.067	0.001
DT	0.9 ±0.1	0.03 ±0.01	94.4 ±1.6	58.7 ±28.3	-173 ±104	-0.462 ±0.093	0.006
Q-DT	1.0 ±0.1	0.00 ±0.00	93.6 ±2.1	20.1 ±21.4	-187 ±113	-0.665 ±0.135	0.010
GNN-DT (Ours)	0.9 ±0.1	0.19 ±0.03	99.3 ±0.2	21.7 ±22.8	-142 ±89	-0.027 ±0.023	0.023
Optimal (Offline)	1.9 ±0.2	1.08 ±0.19	99.1 ±0.2	2.0 ±4.6	-119 ±84	-0.020 ±0.015	-

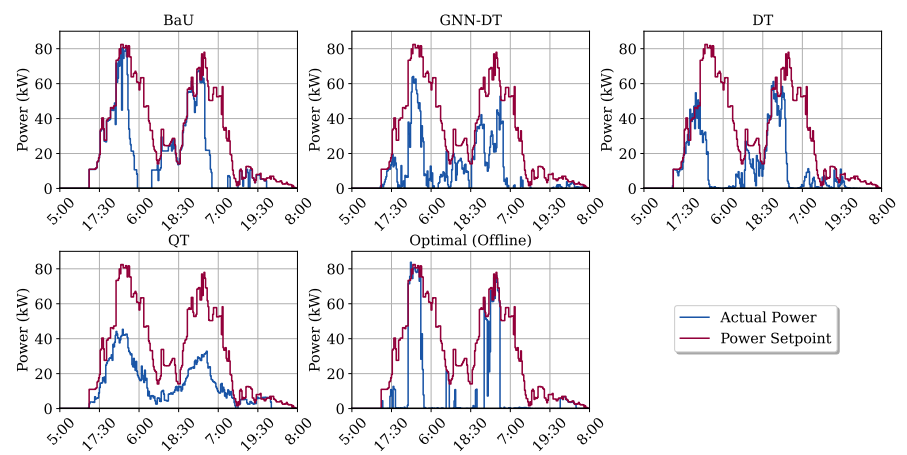
Fig. 6 presents the results from a single evaluation scenario, focusing on the performance of various charging strategies across all 25 charging stations. Fig. 6a illustrates the individual battery trajectories for each EV across the stations, showing how the actual SoC evolves over time. The desired SoC is compared against the results from different algorithms: BaU, GNN-DT, DT, Q-DT, and the Optimal (Offline) solution. It is evident that GNN-DT closely tracks the desired SoC across all stations, outperforming the other methods, particularly in terms of maintaining the target SoC. Fig. 6b provides insights into the aggregate power usage of the entire EV fleet, where the actual power used is compared to the setpoint power. GNN-DT closely aligns with the power setpoint, demonstrating effective power management, while other methods such as BaU and Q-DT show greater deviations, indicating less efficient power usage. These results underline the superior performance of GNN-DT in optimizing charging strategies while adhering to power constraints.

A.5 State Transition Distribution Experiments

To analyze the generalization capability of our model, we examine how it performs under environments with varying state transition probabilities. Specifically, we visualize key environment variables that directly impact the transition dynamics. Figure 7a–d presents the probability distributions of EV arrival time, departure time, duration of stay, and state of SoC at arrival across four scenarios: the original training environment and environments with small, medium, and extreme variations. These plots help quantify the extent of variation in each case. Additionally, Figure 7e illustrates the temporal distribution of the power limit in each scenario, providing further insight into the differences in environment configuration.



(a)



(b)

Figure 6: Complete results for a single evaluation scenario:(a) illustrating individual EV battery trajectories across all 25 charging stations, and (b) presenting the actual aggregate power usage against the power limit for the entire EV fleet.

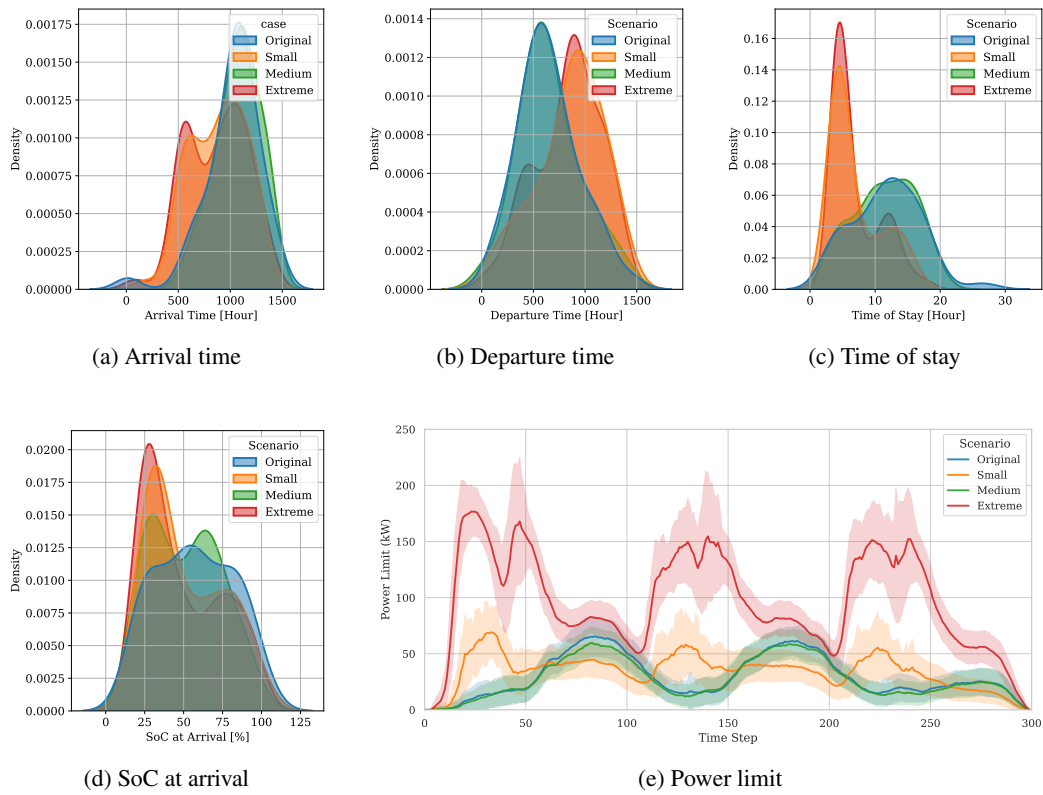


Figure 7: Overview of the five key metrics: (a) arrival time, (b) departure time, (c) power limit, (d) state of charge upon arrival, and (e) time of stay.

B Appendix: Training

Here, we present the hyperparameter settings used for training DT, Q-DT, and GNN-DT, accompanied by detailed training curves that illustrate the convergence of each model.

B.1 Training Hyperparameters

Table 7: Algorithm hyperparameters.

Hyperparameter	Value
Batch Size	64 (for large scale), 128 (for small scale)
Learning Rate	10^{-4}
Weight Decay	10^{-4}
Number of Steps per Iteration	1000
Number of Decoder Layers	3
Number of Attention Heads	4
Embedding Dimension	256
GNN Embedder Feature Dimension	16
GNN Hidden Dimension	32 (for small scale), 64 (for large scale)
Number of GCN Layers	3
Number of Epochs	250 (for small scale), 400 (for large scale)
Number of Steps per Iteration	1000 (for small scale), 3000 (for large scale)
Embedding Dimension	128 (for small scale), 256 (for large scale)
CPU Memory (GB)	8 (for small scale), 16 or 40 (for large scale)
Time Limit (hours)	10 (for small scale), 20 or 46 (for large scale)

B.2 Impact of larger context lengths (K)

Fig. 8 demonstrates that the context length K plays a key role in the performance of GNN-DT, with diminishing returns beyond a certain point. For high-quality datasets like *Optimal*, moderate context lengths ($K = 5$ to $K = 10$) yield the best results, while larger K values do not improve performance significantly. For suboptimal datasets like *BaU* and *Random*, the performance is lower overall, and longer context lengths seem to offer meaningful improvements, particularly when using the *BaU* dataset. Thus, selecting an appropriate context length is crucial for achieving better performance, while the quality of the dataset remains the most influential factor.

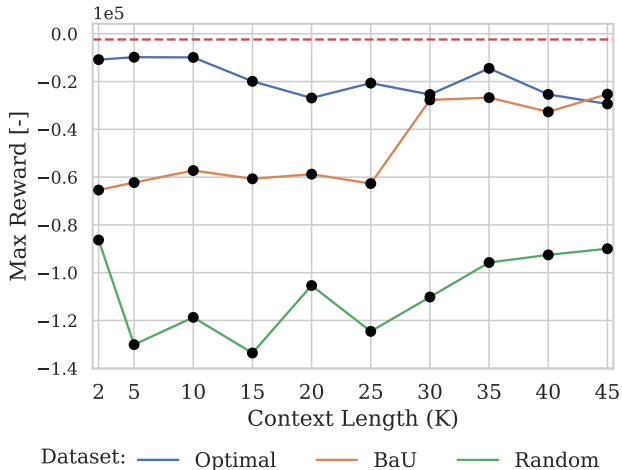


Figure 8: GNN-DT performance for larger context lengths (K).

B.3 Detailed Training Curves

Fig. 9 provides a detailed comparison of training curves for various algorithm-dataset-context length (K) combinations, highlighting the significant impact of the training sample size on performance. The figure includes training results for DT, Q-DT, and GNN-DT across different datasets (Optimal, Random, and BaU) and context lengths ($K = 2$ and $K = 10$), with each plot showing the performance for 100, 1,000, and 10,000 trajectory samples.

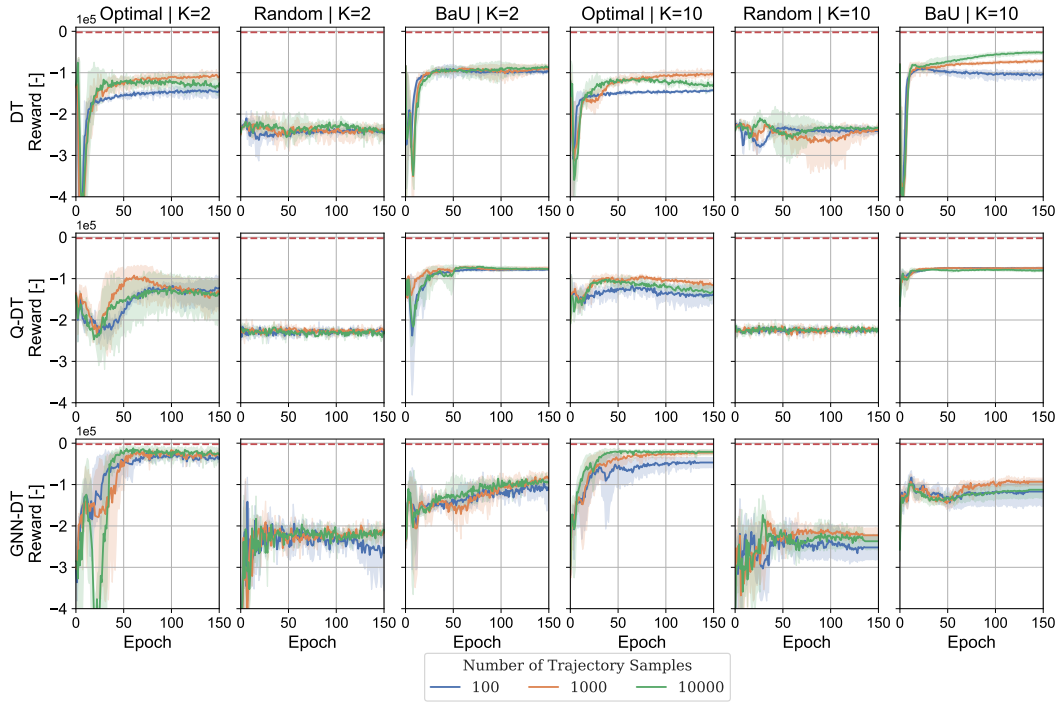


Figure 9: Complete comparison of training curves for combinations of algorithms-K-training dataset for different numbers of samples.

B.4 Mixed Dataset Training Curves

Fig. 10 presents the learning curves for the mixed datasets approach, comparing performance across various combinations of Optimal, Random, and BaU datasets for both $K = 2$ and $K = 10$. Fig. 10a illustrates the results for mixed Optimal datasets, where different proportions of the Optimal and Random datasets (e.g., 50% Optimal + 50% Random) are used for training. The performance becomes more unstable as more Random data is included. Interestingly, the performance for all the mixed datasets demonstrates better maximum reward reached compared to the Optimal-only dataset, highlighting the benefits of combining high-quality and lower-quality data. Fig. 10b and Table 8 shows similar trends for the Mixed-BaU datasets. While the BaU dataset alone performs worse than the Optimal dataset, mixing it with Random data still yields improvements, with the 75% BaU and 25% Random combination showing the best results. The results underscore the potential of mixing datasets to improve training performance, especially when high-quality data (Optimal or BaU) is supplemented with lower-quality Random data.

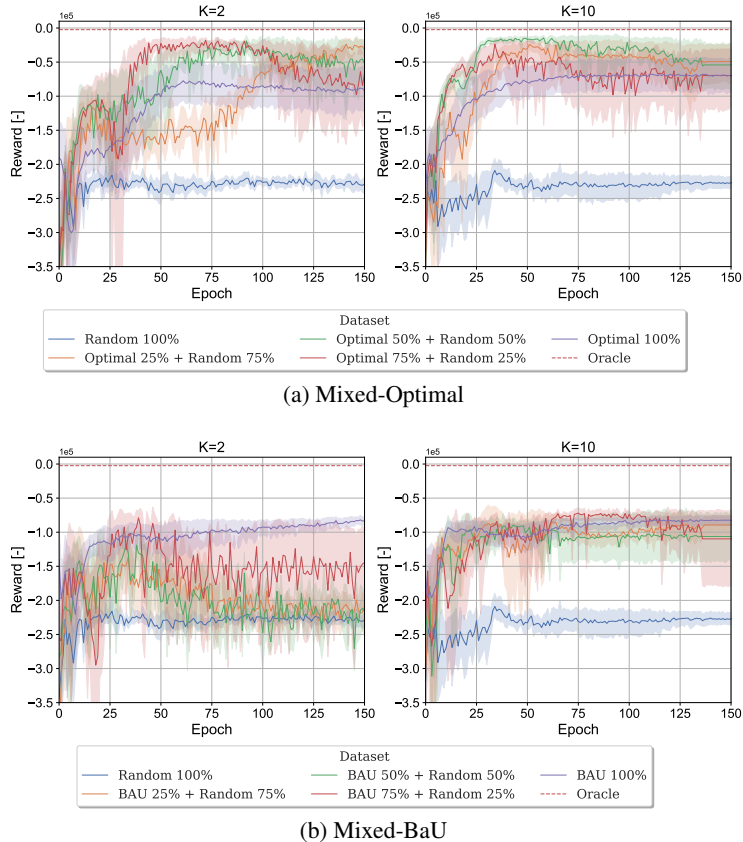


Figure 10: Mixed datasets learning curves for optimal and BaU.

Table 8: Maximum reward of GNN-DT trained on merged BaU-Random datasets for $K = 2$ and $K = 10$. The bold indicates the training dataset with the highest evaluation reward.

Dataset	Total Traj.	Avg. Dataset Reward	GNN-DT Reward ($\times 10^5$)	
			K=2	k=10
Random (Rnd.) 100%	1000	-2.37 ± 0.39	-0.863	-1.187
BaU 25% + Rnd. 75%	1000	-1.93 ± 0.80	-0.578	-0.461
BaU 50% + Rnd. 50%	1000	-1.51 ± 0.87	-0.665	-0.447
BaU 75% + Rnd. 25%	1000	-1.09 ± 0.76	-0.421	-0.471
BaU 100%	1000	-0.01 0.01	-0.654	-0.572